Finding Analytical Solutions to Abundance Fully-Constrained Linear Spectral Mixture Analysis

Hsiao-Chi Li, Meiping Song and Chein-I Chang, *Fellow*, *IEEE*

***Abstract*—This paper revisits a well-known fully constrained least squares (FCLS) method developed by Heinz and Chang and develops an approach to finding analytical solutions to FCLS, called analytical FCLS (AFCLS) which can be solved in closed forms instead of FCLS being solved by numerically algorithms. As a result, the AFCLS-unmixed results using analytical solutions are more accurate than FCLS-unmixed results resulting from numerical solutions.**

***Index Terms*—Analytical FCLS (AFCLS). Fully constrained least squares (FCLS). Modified fully constrained least squares (MFCLS). Non-negativity-constrained least squares (NCLS)**

I. Introduction

Linear spectral mixture analysis (LSMA) is a very useful theory in many applications [1], specifically in linear spectral unmixing (LSU) which assumes that data sample vectors are linearly mixed by a set of so-called, endmembers via a linear mixing model and then unmixes data sample vectors in terms of abundance fractions of these endmembers. In order to fulfill physical constraints, the unmixed abundance fractions must be non-negative and also summed up to one, both of which are referred to as abundance non-negativity constraint (ANC) and abundance sum-to-one constraint (ASC) respectively. One major difficulty with implementing abundance constrained LSMA is the inequality-constraints imposed by ANC which prevents the Lagrange multiplier method from being used to solve problems. In this case, the Kuhn-Tucker conditions must be used instead to develop numerical algorithms to find optimal solutions. Two well-known algorithms to be used for this purpose are an abundance ANC-constrained, called non-negativity constrained least squares (NCLS) method developed by Chang and Heinz in [2] and a fully abundance (ASC, ANC)-constrained, called abundance fully constrained least squares (FCLS) method developed by Heinz and Chang in [3].

H.C. Li is with the Remote Sensing Signal and Image Processing Laboratory, Department of Computer Science and Electrical Engineering, University of Maryland, Baltimore County, Baltimore, MD 21250 USA (e-mail: hsli1@umbc.edu).

M. Song is with Information and Technology College, Dalian Maritime University, 1 Linhai Road, Dalian, China. (e-mail: smping@163.com)

C.-I Chang is with the Remote Sensing Signal and Image Processing Laboratory, Department of Computer Science and Electrical Engineering, University of Maryland, Baltimore County, Baltimore, MD 21250 USA and also with Department of Electrical Engineering, National Chung Hsing University, Taichung, Taiwan, ROC. (e-mail: cchang@umbc.edu).

Since then these algorithms become benchmark algorithms to solve abundance-constrained LSMA (AC-LSMA) problems and many algorithms developed in the literature to solve AC-LSMA are either variants or modifications of FCLS. To the author's best knowledge none of these techniques were able to derive analytical solutions to AC-LSMA. Interestingly, a modified FCLS (MFCLS) which was previously developed in [4-5] and later documented in [1] seems to provide a feasible means of achieving this goal. Despite the fact that the MFCLS was originally developed as an iterative algorithm and did not provide analytic solutions, this paper revisits its approach and actually derives closed forms for AC-LSMA, analytical FCLS (AFCLS). In order to conduct such a comparative quantitatively synthetic image experiments are performed. The experimental results indeed show that AFCLS provides more accurate unmixed results than FCLS and MFCLS do.

II. LSMA

Suppose that L is the number of spectral bands and $\mathbf{r}$ is an L-dimensional image pixel vector. Assume that there are p material substances, $\mathbf{t}_1,\mathbf{t}_2,\cdots,\mathbf{t}_p$ present in an image scene. Let $\mathbf{m}_1,\mathbf{m}_2,\cdots,\mathbf{m}_p$ denote their corresponding substance signatures, which are generally referred to as digital numbers (DN). A linear mixture model of $\mathbf{r}$ models the spectral signature of $\mathbf{r}$ as a linear combination of $\mathbf{m}_1,\mathbf{m}_2,\cdots,\mathbf{m}_p$ with appropriate abundance fractions specified by $\alpha_1,\alpha_2,\cdots,\alpha_p$. More precisely, $\mathbf{r}$ is an $L\times 1$ column vector and $\mathbf{M}$ be an $L\times p$ substance spectral signature matrix, denoted by $\lfloor \mathbf{m}_1\mathbf{m}_2\cdots\mathbf{m}_p \rfloor$, where $\mathbf{m}_j$ is an $L\times 1$ column vector represented by the spectral signature of the j-th substance $\mathbf{t}_j$ resident in the pixel vector $\mathbf{r}$. Let $\boldsymbol{\alpha}=(\alpha_1,\alpha_2,\cdots,\alpha_p)^T$ be a $p\times 1$ abundance column vector associated with $\mathbf{r}$ where α_j denotes the abundance fraction of the j-th substance signature $\mathbf{m}_j$ present in the pixel vector $\mathbf{r}$. In order to restore the pixel vector $\mathbf{r}$, we assume that the spectral signature of the pixel vector $\mathbf{r}$ is linearly mixed by $\mathbf{m}_1,\mathbf{m}_2,\cdots,\mathbf{m}_p$, the spectral signatures of the p substances, $\mathbf{t}_1,\mathbf{t}_2,\cdots,\mathbf{t}_p$ as follows.

$$\mathbf{r}=\mathbf{M}\boldsymbol{\alpha}+\mathbf{n} \tag{1}$$

where $\mathbf{n}$ is noise or can be interpreted as a measurement or model error.

By inspecting (1) the linear model used by LSMA is similar

to a linear model used by Wiener filter except that (1) explores correlation among p substance signatures compared to the latter which uses a linear model to account for p the past observed data samples to perform prediction. Furthermore, by virtue of (1) a hyperspectral image viewed as an image cube can be restored by a set of p abundance fraction maps.

A classical approach to solving (1) is the least squares estimation given by

$$\hat{\boldsymbol{\alpha}}^{\mathrm{LS}}(\mathbf{r}) = \left(\mathbf{M}^T\mathbf{M}\right)^{-1}\mathbf{M}^T\mathbf{r} \tag{2}$$

where $\hat{\boldsymbol{\alpha}}^{\mathrm{LS}}(\mathbf{r}) = \left(\hat{\alpha}_1^{\mathrm{LS}}(\mathbf{r}), \hat{\alpha}_2^{\mathrm{LS}}(\mathbf{r}), \cdots, \hat{\alpha}_p^{\mathrm{LS}}(\mathbf{r})\right)$ and $\hat{\alpha}_j^{\mathrm{LS}}(\mathbf{r})$ is the abundance fraction of the j^{th} substance signature $\mathbf{m}_j$ estimated from the data sample vector $\mathbf{r}$. Here the data sample vector is included to emphasize that the abundance estimate is determined by $\mathbf{r}$.

In order to faithfully restore the spectral information contained in data sample vectors via LSMA three issues need to be addressed. One is determination of the value of p, i.e., number of substance signatures. Another is to find a desired set of p substance signatures, $\mathbf{m}_1, \mathbf{m}_2, \cdots, \mathbf{m}_p$ in an unsupervised manner. The last issue is to impose two physical constraints on model (1), which are abundance sum-to-one constraint (ASC), $\sum_{j=1}^{p}\alpha_j = 1$ and (2) abundance non-negativity constraint (ANC), $\alpha_j \geq 0$ for all $1 \leq j \leq p$. In what follows we will deal with these three issues and provide solution to each of them.

III. Modified Abundance Fully Constrained Methods

For mathematical tractability the solutions given by (2) and (4) are abundance-unconstrained in the sense that no physical constraints are imposed on the model (1). However, in order to restore data integrity to satisfy reality, abundance constraints must be imposed on the substance signatures in (1) by both ASC or ANC on the abundance vector $\boldsymbol{\alpha}$ in (1). The main difficulty with solving constrained linear mixing problems is the constraint of abundance non-negativity that prohibits us from using the Lagrange multiplier method to find solutions analytically. Recently, an alternative approach to the commonly used fully constrained least squares (FCLS) method developed by Heinz and Chang in [3] was developed by Ren and Chang in [4] which replaced ANC with an equivalent constraint. More specifically, instead of directly dealing with the inequalities, $\alpha_j \geq 0$ for each $1 \leq j \leq p$, we replace ANC with an absolute abundance sum-to-one constraint (AASC), $\sum_{j=1}^{p}|\alpha_j| = 1$ which is equivalent to $sign(\boldsymbol{\alpha})^T\boldsymbol{\alpha} = 1$. With AASC coupled with ASC, a modified abundance fully constrained least squares linear mixing problem can be cast as follows.

$$\min_{\boldsymbol{\alpha}\in\boldsymbol{\Delta}}\left\{(\mathbf{r}-\mathbf{M}\boldsymbol{\alpha})^T(\mathbf{r}-\mathbf{M}\boldsymbol{\alpha})\right\} \tag{3}$$

subject to

$$\boldsymbol{\Delta} = \left\{\boldsymbol{\alpha} \mid \sum_{j=1}^{p}\alpha_j = 1 \text{ and } \sum_{j=1}^{p}|\alpha_j| = 1\right\} \tag{4}$$

By introducing two Lagrange multipliers, λ_1 and λ_2 we derive the following objective function

$$\begin{aligned} J(\boldsymbol{\alpha},\lambda_1,\lambda_2) &= (1/2)(\mathbf{r}-\mathbf{M}\boldsymbol{\alpha})^T(\mathbf{r}-\mathbf{M}\boldsymbol{\alpha}) + \lambda_1\left(\sum_{j=1}^{p}\alpha_j - 1\right) \\ &+ \lambda_2\left(\sum_{j=1}^{p}|\alpha_j| - 1\right) \\ &== (1/2)(\mathbf{r}-\mathbf{M}\boldsymbol{\alpha})^T(\mathbf{r}-\mathbf{M}\boldsymbol{\alpha}) + \lambda_1\left(\sum_{j=1}^{p}\alpha_j - 1\right) \\ &+ \lambda_2\left(sign(\boldsymbol{\alpha})^T\boldsymbol{\alpha} - 1\right) \end{aligned} \tag{5}$$

Differentiating (5) with respect to $\boldsymbol{\alpha}$, λ_1 and λ_2 respectively and setting to zero yields

$$\left.\frac{\partial J(\boldsymbol{\alpha},\lambda_1,\lambda_2)}{\partial\boldsymbol{\alpha}}\right|_{\hat{\boldsymbol{\alpha}}^{\mathrm{MFCLS}}(\mathbf{r})} = 0$$

$$\Rightarrow \left(\mathbf{M}^T\mathbf{M}\right)\boldsymbol{\alpha} - \mathbf{M}^T\mathbf{r} + \lambda_1^*\mathbf{1} + \lambda_2^*\left[(sign(\boldsymbol{\alpha})^T\right]_{\boldsymbol{\alpha}=\hat{\boldsymbol{\alpha}}^{\mathrm{MFCLS}}(\mathbf{r})} = 0 \tag{6}$$

$$\left.\frac{\partial J(\boldsymbol{\alpha},\lambda_1,\lambda_2)}{\partial\lambda_1}\right|_{\lambda_1^*} = \mathbf{1}^T\hat{\boldsymbol{\alpha}}^{\mathrm{MFCLS}}(\mathbf{r}) - \mathbf{1} = 0 \tag{7}$$

$$\left.\frac{\partial J(\boldsymbol{\alpha},\lambda_1,\lambda_2)}{\partial\lambda_2}\right|_{\lambda_2^*} = \left(sign(\hat{\boldsymbol{\alpha}}^{\mathrm{MFCLS}}(\mathbf{r}))\right)^T\hat{\boldsymbol{\alpha}}^{\mathrm{MFCLS}}(\mathbf{r}) - \mathbf{1} = 0 \tag{8}$$

which lead to the MFCLS method.

However, using the constraint of $\mathbf{1}^T\hat{\boldsymbol{\alpha}}^{\mathrm{MFCLS}}(\mathbf{r}) = 1$ in (6) we can also derive

$$\begin{aligned} &\mathbf{1}^T\hat{\boldsymbol{\alpha}}^{\mathrm{LS}}(\mathbf{r}) - \left(\lambda_1^*\mathbf{1}^T\left(\mathbf{M}^T\mathbf{M}\right)^{-1}\mathbf{1} + \lambda_2^*\mathbf{1}^T\left(\mathbf{M}^T\mathbf{M}\right)^{-1}\mathbf{b}\right) = 1 \\ &\Rightarrow \lambda_1^*\mathbf{1}^T\left(\mathbf{M}^T\mathbf{M}\right)^{-1}\mathbf{1} + \lambda_2^*\mathbf{1}^T\left(\mathbf{M}^T\mathbf{M}\right)^{-1}\mathbf{b} = \left(\mathbf{1}^T\hat{\boldsymbol{\alpha}}^{\mathrm{LS}}(\mathbf{r}) - 1\right) \end{aligned} \tag{9}$$

and using the constraint of $\mathbf{b}^T\hat{\boldsymbol{\alpha}}^{\mathrm{MFCLS}}(\mathbf{r}) = 1$ in (9) we can further imply

$$\begin{aligned} &\mathbf{b}^T\hat{\boldsymbol{\alpha}}^{\mathrm{LS}}(\mathbf{r}) + \mathbf{b}^T\left(\mathbf{M}^T\mathbf{M}\right)^{-1}\left(\lambda_1^*\mathbf{1} + \lambda_2^*\mathbf{b}\right) = 1 \\ &\Rightarrow \lambda_1^*\mathbf{b}^T\left(\mathbf{M}^T\mathbf{M}\right)^{-1}\mathbf{1} + \lambda_2^*\mathbf{b}^T\left(\mathbf{M}^T\mathbf{M}\right)^{-1}\mathbf{b} = \left(\mathbf{b}^T\hat{\boldsymbol{\alpha}}^{\mathrm{LS}}(\mathbf{r}) - 1\right) \\ &\Rightarrow \lambda_1^*\mathbf{b}^T\mathbf{a} + \lambda_2^*\mathbf{b}^T\mathbf{c} = \left(\mathbf{b}^T\hat{\boldsymbol{\alpha}}^{\mathrm{LS}}(\mathbf{r}) - 1\right) \end{aligned} \tag{10}$$

where $\mathbf{a} = \left(\mathbf{M}^T\mathbf{M}\right)^{-1}\mathbf{1}$ and $\mathbf{c} = \left(\mathbf{M}^T\mathbf{M}\right)^{-1}\mathbf{b}$. As a result, (9) and (10) become

$$\lambda_1^*\mathbf{1}^T\mathbf{a} + \lambda_2^*\mathbf{1}^T\mathbf{c} = \left(\mathbf{1}^T\hat{\boldsymbol{\alpha}}^{\mathrm{LS}}(\mathbf{r}) - 1\right) \tag{11}$$

$$\lambda_1^*\mathbf{b}^T\mathbf{a} + \lambda_2^*\mathbf{b}^T\mathbf{c} = \left(\mathbf{b}^T\hat{\boldsymbol{\alpha}}^{\mathrm{LS}}(\mathbf{r}) - 1\right). \tag{12}$$

The solution to solving (11) and (12) can be simultaneously solved for λ_1 and λ_2 by

$$\lambda_1^* = \frac{\begin{vmatrix}\left(\mathbf{1}^T\hat{\boldsymbol{\alpha}}^{\mathrm{LS}}(\mathbf{r}) - 1\right) & \mathbf{1}^T\mathbf{c} \\ \left(\mathbf{b}^T\hat{\boldsymbol{\alpha}}^{\mathrm{LS}}(\mathbf{r}) - 1\right) & \mathbf{b}^T\mathbf{c}\end{vmatrix}}{\begin{vmatrix}\mathbf{1}^T\mathbf{a} & \mathbf{1}^T\mathbf{c} \\ \mathbf{b}^T\mathbf{a} & \mathbf{b}^T\mathbf{c}\end{vmatrix}}, \quad \lambda_2^* = \frac{\begin{vmatrix}\mathbf{1}^T\mathbf{a} & \left(\mathbf{1}^T\hat{\boldsymbol{\alpha}}^{\mathrm{LS}}(\mathbf{r}) - 1\right) \\ \mathbf{b}^T\mathbf{a} & \left(\mathbf{b}^T\hat{\boldsymbol{\alpha}}^{\mathrm{LS}}(\mathbf{r}) - 1\right)\end{vmatrix}}{\begin{vmatrix}\mathbf{1}^T\mathbf{a} & \mathbf{1}^T\mathbf{c} \\ \mathbf{b}^T\mathbf{a} & \mathbf{b}^T\mathbf{c}\end{vmatrix}} \tag{13}$$

which are not derived in any literature. Accordingly, $\hat{\boldsymbol{\alpha}}^{\mathrm{MFCLS}}(\mathbf{r})$ specified by (6) can be obtained analytically by finding $\hat{\boldsymbol{\alpha}}^{\mathrm{LS}}(\mathbf{r})$ via (2) and λ_1^* and λ_2^* via (13) simultaneously to solve an optimal set of the p-dimensional abundance vector $\boldsymbol{\alpha}$, λ_1 and λ_2 altogether using the following simultaneously algebraic equations

$$\begin{bmatrix} \left(\mathbf{M}^T\mathbf{M}\right)\boldsymbol{\alpha} - \mathbf{M}^T\mathbf{r} + \lambda_1\mathbf{1} + \lambda_2 sign(\boldsymbol{\alpha}) \\ \left(sign(\boldsymbol{\alpha}(\mathbf{r}))\right)^T \boldsymbol{\alpha}(\mathbf{r}) \\ \mathbf{1}^T\boldsymbol{\alpha}(\mathbf{r}) \end{bmatrix} = \begin{bmatrix} \mathbf{0}_{p\times 1} \\ 1 \\ 1 \end{bmatrix} \tag{14}$$

which leads to analytical FCLS (AFCLS). The key difference between MFCLS and AFCLS is that the former assumes its initial abundance estimator already satisfies ASC and then finds iterative solutions via (8) compared to the latter which actually solves all the three equations specified by (14). Consequently, AFCLS is in fact the one which produces the optimal solutions as opposed to suboptimal solutions produced by FCLS and MFCLS.

IV. Real Image Experiments

The image scene shown in Fig. 4 was acquired by the airborne Hyperspectral Digital Imagery Collection Experiment (HYDICE) sensor in August 1995 from a flight altitude of 10000 ft with ground sampling distance approximately 1.5 m.

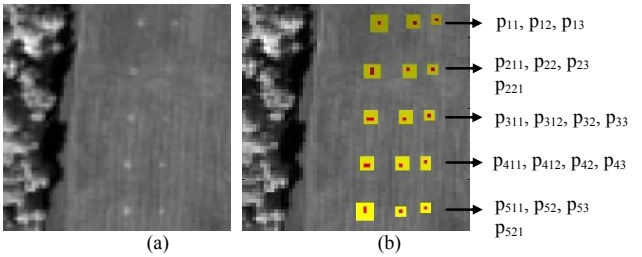

Figure 1. (a) A HYDICE panel scene which contains 15 panels; (b) Ground truth map of spatial locations of the 15 panels

It has 210 spectral channels ranging from 0.4 μm to 2.5 μm with spectral resolution is 10 nm. The low signal/high noise bands: bands 1-3 and bands 202-210; and water vapor absorption bands: bands 101-112 and bands 137-153, were removed. So, a total of 169 bands were used for the experiments. It has size of 64×64 pixel vectors shown in Fig. 1(a) along with its ground truth provided in Fig. 1(b) is used for experiments where the center and boundary pixels of objects are highlighted by red and yellow respectively. Each element in Fig. 1(b) is a square panel and denoted by p_{ij} with rows indexed by $i = 1,2,\cdots,5$ and columns indexed by $j = 1,2,3$.

Within the scene in Fig. 1(a) there is a large grass field and a forest on the left edge. Each element in this matrix is a square panel and denoted by p_{ij} with rows indexed by i and columns indexed by $j = 1,2,3$. For each row $i = 1,2,\cdots,5$, there are three panels painted by the same paint but with three different sizes. The sizes of the panels in the first, second and third columns are $3\text{m}\times 3\text{m}$ and $2\text{m}\times 2\text{m}$ and $1\text{m}\times 1\text{m}$ respectively. Since the size of the panels in the third column is $1\text{m}\times 1\text{m}$, they cannot be seen visually from Fig. 10(a) because of their size less than the 1.56m pixel resolution. For each column $j = 1,2,3$, the 5 panels have same sizes but in five different paints. However, it should be noted that the panels in rows 2 and 3 were made by the same material with two different paints. Similarly, it is also the case for panels in rows 4 and 5. Nevertheless, they were still considered as different panels but our experiments will demonstrate that detecting panels in row 5 (row 3) may also have effect on detection of panels in row 4 (row 2). The 1.56m-spatial resolution of the image scene suggests that most of the 15 panels are one pixel in size except that the panels in the 1st column with the 2nd, 3rd, 4th, 5th rows which are two-pixel panels, denoted by p_{211}, p_{221}, p_{311}, p_{312}, p_{411}, p_{412}, p_{511}, p_{521}. As a result, there are a total 19 panel pixels. Fig. 10(b) shows the precise spatial locations of these 19 panel pixels where red pixels (R pixels) are the panel center pixels and the pixels in yellow (Y pixels) are panel pixels mixed with the BKG. Fig. 10(c) shows the spectra of five panel signatures $\mathbf{p}_1$, $\mathbf{p}_2$, $\mathbf{p}_3$, $\mathbf{p}_4$, $\mathbf{p}_5$ obtained by averaging the center R panel pixels for each of five rows. Also, 1.56m-spatial resolution can be used to calculate the size of panel pixels in the 2nd column to be $1/(1.56)^2 \approx 0.4$.

According to the ground truth the five panel signatures were obtained by the R pixels in the 1st and 2nd columns, i.e., each panel signature was obtained by averaging the R pixels in the 1st and 2nd columns in a particular row and the other four BKG signatures were obtained by prior knowledge as the areas marked in Fig. 2 as interferer, tree, grass, road to make up 5 target classes representing five panel signatures and 4 BKG signatures.

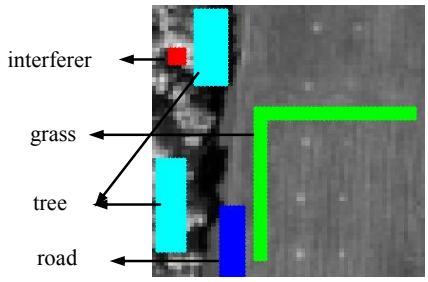

Figure 2. Four BKG classes obtained by marked areas

Table 1 tabulates the unmixed abundance fractions of 19 panel pixels by the three unmixing methods, FCLS, MFCLS and AFCLS where the unmixed results for 4 BKG classes were not displayed because the BKG classes were not of major interest and the pixel size calculated from the ground truth is also provided in the 2nd column.

Table 2. Unmixed abundance fractions of 19R pixels by FCLS, MFCLS and AFCLS

		FCLS	MFCLS	AFCLS
Computing time		0.0217	0.0154	3.0554
panel pixels	ground truth			
p_{11}	1	0.7948	0.7617	0.6488
p_{12}	1	0.5541	0.5549	0.5126
p_{13}	0.4	0.0367	0.0355	0.0009
p_{211}	1	0.5734	0.5436	0.5714
p_{212}	1	0.9163	0.9156	0.7865
p_{22}	1	0.8827	0.8828	0.8660
p_{23}	0.4	0.4666	0.4670	0.4012
p_{311}	1	0.9142	0.9136	0.9002
p_{312}	1	0.9068	0.9025	0.8814
p_{32}	1	0.6521	0.6647	0.5802

p_{33}	0.4	0.2103	0.2105	0.2111
p_{411}	1	0.5481	0.5094	0.4456
p_{412}	1	0.4375	0.4378	0.4294
p_{42}	1	0.6956	0.6910	0.6288
p_{43}	0.4	0.1577	0.1572	0.1036
p_{511}	1	0.8304	0.8304	0.8201
p_{521}	1	1.0119	1.0000	1.0000
p_{52}	1	0.9354	0.9353	0.9360
p_{53}	0.4	0.1377	0.1374	0.1137
Least squares errors		7.1121E+02	7.4680E+02	7.5832E+02

Interestingly, the results in Table 1 show that FCLS produced the minimum least squares error, while MFCLS required the least computing time and AFCLS was the worst one. But this was mainly due to the fact that the prior knowledge which used 9 signatures to produce the results in Table 1 was generally not sufficient as shown in [3]. So, we used automatic target generation process (ATGP) developed in [7] to generate 34 target pixels shown in Fig. 3 which were used to form a linear mixing model to perform LSMA.

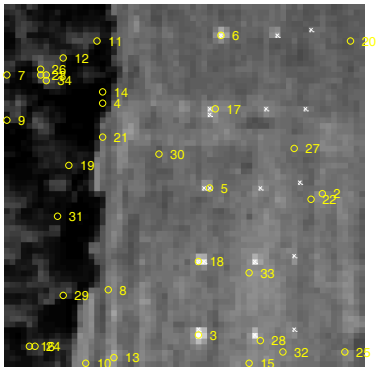

Figure 3. 34 ATGP-generated target pixels

Table 2 tabulates the unmixed abundance fractions of 19 panel pixels by the three unmixing methods, FCLS, MFCLS and AFCLS where the same conclusions made for Table 1 were true. However, if we look into individual R panel pixels, AFCLS actually produced better accuracy for most panel pixels.

Table 2. Unmixed abundance fractions of 19R pixels by FCLS, MFCLS and AFCLS using 34 target signatures generated by ATGP in Fig. 3

		FCLS	MFCLS	AFCLS
Computing time		0.0233	0.0187	3.1359
panel pixels	ground truth			
p_{11}	1	1.0000	1.0000	1.0000
p_{12}	1	0.3748	0.3747	0.3828
p_{13}	0.4	0.0320	0.0319	0.0091
p_{211}	1	0.5061	0.5053	0.5078
p_{212}	1	1.0000	1.0000	1.0000
p_{22}	1	0.6646	0.6646	0.6655
p_{23}	0.4	0.3457	0.3457	0.3558
p_{311}	1	0.8631	0.8631	0.8654
p_{312}	1	1.0000	1.0000	1.0000
p_{32}	1	0.5319	0.5317	0.5263
p_{33}	0.4	0.3461	0.3461	0.3520
p_{411}	1	1.0000	1.0000	1.0000
p_{412}	1	0.3578	0.3578	0.3872
p_{42}	1	0.7095	0.7095	0.7102
p_{43}	0.4	0.2345	0.2345	0.1825
p_{511}	1	0.7245	0.7245	0.7242
p_{521}	1	1.0000	1.0000	1.0000
p_{52}	1	0.7773	0.7773	0.7767
p_{53}	0.4	0.1508	0.1508	0.1519
Least squares errors		2.0153E+02	2.0160E+02	2.0510E+02

VI. Conclusion

Abundance fully constrained linear spectral mixture analysis (AFC-LSMA) generally requires numerical solutions since there is no analytical solutions due to a set of inequalities imposed by non-negativity constraints. This paper develops a theory, analytical FCLS for solving AFC-LSMA problems analytically. Its idea is to replace inequalities imposed by ANC with equality imposed by AASC so that Kuhn-Tucker conditions used to constrain ANC can be actually solved by the Lagrange multiplier method to derive analytical solutions. In this case numerical solutions solved by FCLS can be replaced with analytical solutions by AFCLS solving a set of algebraic equations simultaneously.

References

[1] C.-I Chang, *Hyperspectral* Imaging, Kluwer, N.J., 2003

[2] C.-I Chang and D. Heinz, "Constrained subpixel detection for remotely sensed images," *IEEE Trans. on Geoscience and Remote Sensing*, vol. 38, no. 3, pp. 1144-1159, May 2000.

[3] D. Heinz and C.-I Chang, "Fully constrained least squares linear mixture analysis for material quantification in hyperspectral imagery," *IEEE Trans. on Geoscience and Remote Sensing*, vol. 39, pp. 529-545, 2001.

[4] H. Ren and C.-I Chang, "A constrained least squares approach to hyperspectral image classification," *1999 Conference on Information Science and Systems*, Johns Hopkins University, Baltimore, MD, March 17-19, 1999.

[5] E. Wong and C.-I Chang, "Modified full abundance-constrained spectral unmixing," Proceedings of *Conference High-Performance Computing in Remote Sensing*, SPIE 8539, Edinburgh United Kingdom, 24-27 September, 2012.

[6] C.-I Chang, *Hyperpscetral Data Processing*, Chapter 4, Wiley, 2013.

[7] H. Ren and C.-I Chang, "Automatic spectral target recognition in hyperspectral imagery," *IEEE Trans. on Aerospace and Electronic Systems*, vol. 39, no. 4, pp. 1232-1249, October 2003.